



Molecular dynamics study on flow structure inside a thermal transpiration flow field

Cite as: Phys. Fluids **33**, 012005 (2021); <https://doi.org/10.1063/5.0034146>

Submitted: 20 October 2020 • Accepted: 16 December 2020 • Published Online: 08 January 2021

 Hiroki Yamaguchi (山口浩樹) and  Gota Kikugawa (菊川豪太)

COLLECTIONS

Paper published as part of the special topic on [Advances in Micro/Nano Fluid Flows: In Memory of Prof. Jason Reese](#)



View Online



Export Citation



CrossMark

ARTICLES YOU MAY BE INTERESTED IN

[A depth-averaged model for Newtonian fluid flows in shallow microchannels](#)

Physics of Fluids **33**, 012002 (2021); <https://doi.org/10.1063/5.0035167>

[Flow boiling pressure drop characteristics in a multi-microchannel heat sink](#)

Physics of Fluids **33**, 012004 (2021); <https://doi.org/10.1063/5.0036615>

[Physics guided machine learning using simplified theories](#)

Physics of Fluids **33**, 011701 (2021); <https://doi.org/10.1063/5.0038929>

Physics of Fluids

SPECIAL TOPIC: Flow and Acoustics of Unmanned Vehicles

Submit Today!



Molecular dynamics study on flow structure inside a thermal transpiration flow field

Cite as: Phys. Fluids 33, 012005 (2021); doi: 10.1063/5.0034146

Submitted: 20 October 2020 • Accepted: 16 December 2020 •

Published Online: 8 January 2021



Hiroki Yamaguchi (山口浩樹)^{1,a)}  and Gota Kikugawa (菊川豪太)² 

AFFILIATIONS

¹Department of Micro-Nano Mechanical Science and Engineering, Nagoya University, Furo-cho, Chikusa, Nagoya, Aichi 464-8603, Japan

²Institute of Fluid Science, Tohoku University, 2-1-1 Katahira, Aoba-ku, Sendai, Miyagi 980-8577, Japan

Note: This paper is part of the Special Topic, Advances in Micro/Nano Fluid Flows: In Memory of Prof. Jason Reese.

a) Author to whom correspondence should be addressed: hiroki@nagoya-u.jp

ABSTRACT

Thermal transpiration flow is a thermally driven flow from a cold part toward a hot part using a temperature gradient along a wall under a high Knudsen number condition. Many studies have used this type of flow as a pump for microtechnology. The flows adopted in these studies were, in most cases, in the slip or transitional regime. Accordingly, in this research, thermal transpiration flow through a two-dimensional channel with nanoscale clearance in the height direction was studied using the molecular dynamics method. The solid atoms composing the channel walls were explicitly considered. The center part of the nanochannel was controlled as a hot reservoir, whereas both ends of the nanochannel were kept cold. The temperatures of the channel wall atoms were also controlled based on their positions by linearly interpolating the temperature between the hot and cold reservoirs. Two Knudsen number conditions were adopted by changing the width of the computational cell. To study the mean velocity distribution inside the nanochannel, these simulations were performed for 10 ns. We successfully obtained a mean velocity distribution inside the nanochannel, showing the thermal transpiration flow in the vicinity of the channel wall using the pressure-driven counterflow at the center in the height direction even under the dense gas condition. The velocity profile across the nanochannel in the height direction indicated that thermal transpiration flow was induced in the adsorption layer of gas molecules on the channel wall under the dense gas condition.

Published under license by AIP Publishing. <https://doi.org/10.1063/5.0034146>

I. INTRODUCTION

Gas transport in micro- and nanoscale is important and has attracted attention to enhance the usage of microelectromechanical systems (MEMS).¹ In such small scales, the Knudsen number, which is the ratio of the mean free path of gas molecules to the characteristic length of a system, becomes large, and the effect of rarefaction appears in the flow. Several phenomena are peculiar to a high Knudsen number flow of which thermal transpiration flow is a typical example. Thermal transpiration flow is induced by a temperature gradient along a wall in a cold to hot direction.^{2,3} This flow is driven only by thermal energy. Based on this feature, this type of flow has been studied for realizing a thermal molecular pump (e.g., the Knudsen pump and the accommodation pump).^{4–6} Such pumps do not have mechanical moving

parts and thus are suitable for the application of miniaturization to MEMS.^{7,8}

Research on thermal transpiration flow is important not only for the development of a gas transport system in the microscale but also for better understanding the flow characteristics in the high Knudsen number regime because it represents a basic problem in a high Knudsen number flow. This phenomenon is based on gas-surface interaction and a nonisothermal problem; thus, several factors affect this complicated problem. It has long been investigated both experimentally and numerically. For experimental studies, thermal transpiration flow is induced in a channel connecting two chambers with different temperatures, resulting in a pressure difference between the two chambers. The pressure difference or the ratio of the final equilibrium state^{9–11} and the mass flow rate^{10–13} is measured. Many numerical studies with various approaches have

also been conducted to evaluate the pressure difference and flow rate.^{14–19} The macroscopic characteristics of a flow have also been investigated; however, a detailed study on thermal transpiration flow at the molecular scale is still needed. Furthermore, flows were, in most study cases, used between the continuum flow and free molecular flow regimes, where theoretical analysis is difficult to apply. Since the flow is an inherently molecular motion induced by a gas–surface interaction, it is interesting to investigate the behavior of gas molecules, particularly within the vicinity of solid surfaces.

In this study, the molecular dynamics (MD) simulation is used to investigate the relationship between the velocity field and number density distribution inside thermal transpiration flow. Since molecules adsorb to and migrate on a surface, the flow structure will be affected by the existence of channel wall atoms, which has not been considered in previous studies.^{20,21} The flow inside a nanochannel with a temperature gradient along the channel wall is studied here by explicitly considering the solid atoms of the channel wall to study the behavior of gas molecules near the wall surface.

II. MD SIMULATION

To investigate the thermal transpiration flow in a channel induced by a temperature gradient along a channel wall, a gaseous flow in a nanochannel was simulated using the MD method. The flow through a nanochannel was modeled using the two-dimensional (2D) flow between infinite parallel plates with nanometer-scale clearance. To study the behavior of gas molecules around the wall surface with thermal fluctuations, the solid atoms comprising the channel walls were explicitly considered. The peachgk_md (v.2.141) in-house simulation package was used for which we implemented several additional procedures to simulate thermal transpiration flow. The velocity Verlet algorithm was used for time integration using a time step of 1 fs. To reduce statistical uncertainty, we performed the simulation for 11×10^6 steps, i.e., 11 ns. The data of the initial 10^6 steps (1 ns) were discarded to sample under steady-state conditions of 10^7 steps (10 ns).

Argon was used as a gas species and platinum as the solid material of the channel wall. The channel surface had a (111) surface and was modeled as atomically flat and clean. For the potential models between atoms, the Lennard-Jones (12–6) potential was applied using the parameters $\sigma = 0.247$ nm and $\epsilon = 31.36$ kJ/mol for Pt–Pt interaction, $\sigma = 0.340$ nm and $\epsilon = 0.996$ kJ/mol for Ar–Ar interaction, and $\sigma = 0.294$ nm and $\epsilon = 0.658$ kJ/mol for

Ar–Pt interaction.²² The Ar and Pt masses were $m = 39.95$ amu and 195.1 amu, respectively.

Periodic boundary conditions were applied in all x , y , and z directions. The schematic of the computational cell is shown in Fig. 1. The length of the channel was $L = 55.4$ nm. The channel walls were explicitly modeled by three layers comprised of the outermost fixed, the middle temperature controlled, and the innermost free moving atomic layers. For the channel height, the distance between the innermost atomic layers of the channel walls in contact with gas molecules was $H = 3$ nm, and a vacuum layer with $h_v = 10$ nm was prepared outside of the channel to avoid interaction in the height direction. The width of the computational cell W was varied to control the number of gas molecules N to realize similar statistical errors with different Knudsen number Kn conditions, which was inversely proportional to rarefaction parameter δ . We chose two conditions, i.e., $W = 20.2$ nm (case A) and 50.4 nm (case B). Each top and bottom channel wall comprised three layers of 16 800 and 42 000 solid atoms per layer for cases A and B, respectively. We used 21 950 gas molecules for case A and 18 275 for case B. The Knudsen number Kn is defined by the ratio of the mean free path λ to the channel height H . If we assume gas molecules as hard spheres having a diameter of Lennard-Jones potential parameter σ ,

$$Kn = \frac{\lambda}{H} = \frac{WL}{\sqrt{2}N\sigma^2}, \quad (1)$$

where the channel volume was evaluated using only the geometrical shape of the void space between the two innermost layers of the parallel walls, neglecting the region where gas molecules could not be reached because of excluding volume interaction from the wall atoms. The calculated Kn values were 0.099 for case A and 0.30 for case B. The rarefaction parameter δ is defined via equivalent free path l as follows:³

$$\delta = \frac{H}{l} = \frac{Hp}{\mu\sqrt{\frac{2kT}{m}}} = \frac{N\sqrt{mkT}}{\sqrt{2}\mu WL}, \quad (2)$$

where p , μ , k , T , and m are the pressure, viscosity coefficient, Boltzmann constant, temperature, and mass of gas molecules, respectively; pressure p is estimated using the equation of state for an ideal gas. Since there is a temperature distribution, mean temperature $T_m = 300$ K was used to roughly estimate the mean condition. The rarefaction parameter δ values were 10 for case A and 3.4 for case B. Increasing Kn or decreasing δ by retaining N was difficult for case B

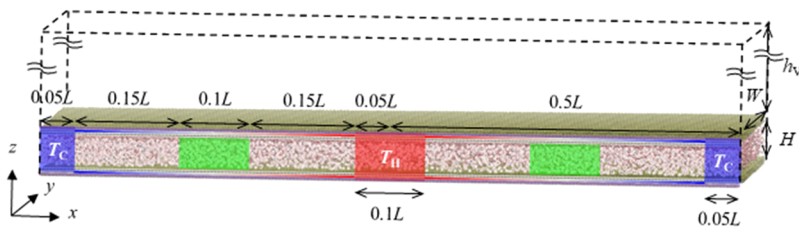


FIG. 1. A schematic of the computational cell with the temperature-controlled areas, where L , W , and H denote the channel length, width, and height, respectively. h_v denotes the height of the vacuum layer.

because we required a large number of solid atoms with an increase in W . The mean molecular spacing under these simulated conditions was calculated as 0.53 nm for case A and 0.77 nm for case B. The simulated flows inside the nanochannel were under the dense gas condition.

To induce thermal transpiration flow, a temperature gradient was applied to the channel wall along the longitudinal direction by controlling the temperatures of the wall atoms and gas molecules in specific areas. A schematic of the temperature-controlled areas is shown in Fig. 1, visualized using Visual Molecular Dynamics (ver. 1.9.3).²³ Since the periodic boundary condition was applied to the longitudinal direction, both ends of the channel were set to the cold temperature, $T_C = 250$ K, as the cold area, with a length of $0.05L$, and the center had a hot temperature, $T_H = 350$ K, as the hot area, with a length of $0.1L$. The temperatures of these areas were controlled using a Langevin thermostat throughout the simulation time. At the channel wall, the temperature of the solid atom was controlled depending on its position. The temperature condition was linearly interpolated between the cold and hot areas. The channel wall was modeled by three atomic layers: the outermost layer, which was farthest from the gas molecules, was fixed to retain the channel position throughout the simulation; the atoms of the middle layer were controlled using the velocity scaling method at a temperature condition based on their position; and the innermost layer, which interacted with gas molecules, moved freely without any control. Accordingly, there were two face-to-face flows directed toward the center of the nanochannel in the simulation. To sample the data for the thermal transpiration flow, the sampling area of the $0.1L$ length was set at the center part of each flow, i.e., the $1/4L$ and $3/4L$ points from the left end.

The initial positions of the gas molecules are typically distributed in a channel randomly, as in the literature.^{15,16} However, there was a temperature distribution in the flow field in this study, and the uniform molecular distribution, i.e., the number density $n = \text{constant}$, led to the pressure distribution, which can be understood from the equation of state for an ideal gas, i.e., $p = nkT$, where the pressure and the Boltzmann constant were expressed as p and k , respectively. The initial pressure distribution induced a pressure-driven flow inside the nanochannel. Even though an early stage of the simulation was discarded to investigate the steady state of the thermal transpiration flow, the pressure-driven flow could last for a

long period and can affect the flow properties. To prevent the initial pressure distribution, we created a nonuniform number density distribution. Initially, gas molecules were randomly dispersed in the flow field so that the number of gas molecules was inversely proportional to the temperature, depending on the wall temperature at its x -position using the rejection sampling method.

III. RESULTS AND DISCUSSION

A. Boundary and initial conditions

Before conducting detailed analyses on thermal transpiration flow inside a microchannel, we first verified our initial and boundary conditions because they were unique settings.

We first checked the temperature distribution of the wall atoms, which is a boundary condition at the microchannel wall. As mentioned in Sec. II, the temperature control was applied to the middle layers of the wall atoms throughout the simulation, whereas the outermost layers of the solid walls were fixed. As such, it was important to check the temperature distribution of the innermost layers of the wall atoms, which directly acted as a boundary condition. The temperature distributions of the wall atoms are shown in Fig. 2 by dividing wall atoms into 20 segments in the longitudinal direction as the sampling areas. We sampled the data for 10 ns with gas molecules inside the channel. Symmetrical temperature gradients are present along the wall in the longitudinal direction. The profiles of the upper and lower walls are also symmetrical. The temperature of the innermost layers is slightly lower than that of the temperature-controlled middle layers, but both temperatures are nonetheless similar. Therefore, we confirmed the temperature gradient along the channel wall according to our expectations.

Next, we checked the effectiveness of the initial nonuniform distribution of gas molecules. The temperature and density distributions were calculated using the data of the initial 10 000 steps to reduce statistical scattering and to obtain meaningful data. We also calculated the product of number density and temperature, i.e., nT , which would be proportional to pressure, based on the equation of state for an ideal gas. Our concept was to reduce the pressure distribution inside the field with temperature distribution. To check the effect of the initial condition, we also plotted this “effective” pressure

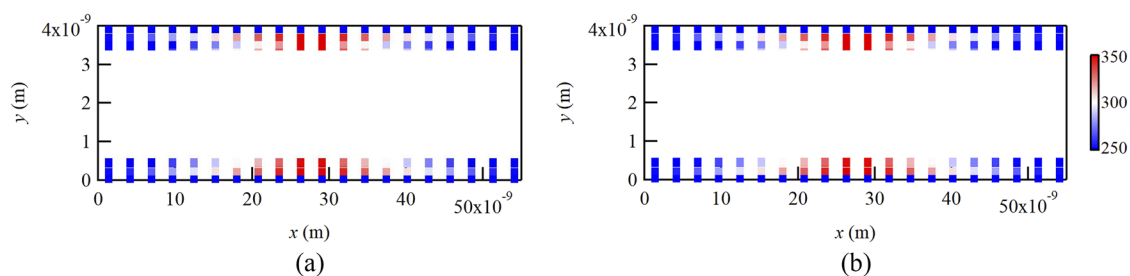


FIG. 2. The temperature distribution of the wall atoms for (a) case A and (b) case B. The vertical axis is enlarged five times compared with the horizontal axis because of the small height-to-length ratio of the channel.

distribution. The effective pressure was normalized by its mean value to clearly show the distribution. The inside of the microchannel was divided by almost 0.5 nm square meshes to obtain the distribution. The temperature, relative number density, and relative effective pressure distributions are shown in Fig. 3. Figure 3(A) shows the temperature in a convex shape in the longitudinal direction as expected. The distribution has an hourglass shape for the x - y plot,

which is consistent with the temperature of the wall atoms in Fig. 2. The number density is almost inversely proportional to the temperature distribution in Fig. 3(B). The number density appeared to be small in the vicinity of the walls because of the region where gas molecules suffered a repulsive force from the wall atoms. If the initial positions of the gas molecules are randomly distributed in the microchannel without considering the temperature distribution, the

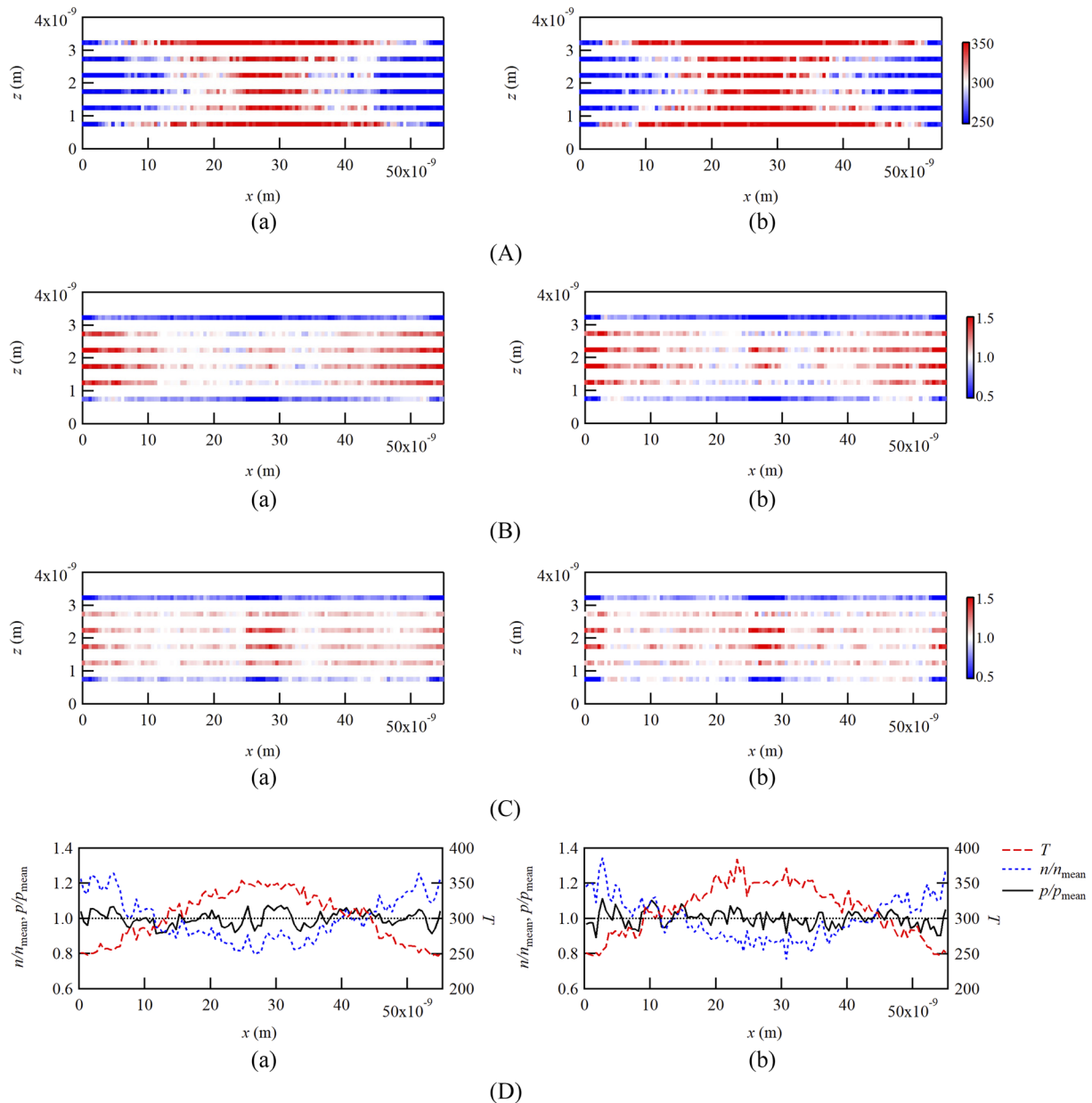


FIG. 3. Distributions inside the nanochannel based on initial conditions for (a) case A and (b) case B: (A) temperature, (B) relative number density normalized by the mean, and (C) relative effective pressure normalized by the mean. The cross-sectional averaged profiles of these three properties are plotted in (D).

effective pressure distribution will be similar to the temperature distribution because it is a product of uniform number density and temperature. It is shown that the uniformity of effective pressure is better in Fig. 3(C). These distributions are averaged over the cross-sectional area to see their one-dimensional profiles in the longitudinal direction, as in Fig. 3(D). The number density profile clearly shows the opposite tendency to the temperature profile, resulting in the almost flat profile of the effective pressure. Thus, the initial distribution was considered to not be significantly different from the steady-state conditions, reducing the number of steps in the initial preparation phase.

B. Mean velocity distribution and profile across the microchannel

The mean velocity vector distribution inside the microchannel, which is difficult to measure in experiments, is shown in Fig. 4. Even though we sampled for 10 ns with 1 fs time steps using approximately 20 000 molecules, scattering of velocity vectors occurred in terms of size and direction. To gain an idea of the thermal transpiration flow, the temperature distribution was also plotted in color contour lines in the range of 250 K–350 K. As explained in Sec. III A, the temperature of the wall was slightly lower than expected. For both rarefaction cases, there were flows in the direction from cold to hot in the vicinity of the walls, i.e., thermal transpiration flow, even under the dense gas condition. Meanwhile, there were counter flows from hot to cold at the center part in the height direction of the microchannel to compensate for thermal transpiration flows near the walls. This flow may be a pressure-driven counterflow, indicating

parabolic profiles. Despite using atomically flat and clean surfaces as channel walls, we observed strong thermal transpiration flows. To check the mass balance of the flows in the nanochannel, the product of the number density and x -component velocity is shown in Fig. 5. It is easily observed that the flow field is mirror symmetric. There are mass flows with large absolute values only in the vicinity of the walls and with the opposite sign with a small absolute value across most part of the nanochannel. The cross-sectional averaged values are almost zero over the entire longitudinal direction of the nanochannel, and the deviations from zero were less than 0.8% of the maximum value.

To observe the profiles in detail, we sampled the velocity and number density profiles in the entirety of two sampling areas shown in Fig. 1. Since the flow field is symmetrical across $x = 0.5L$ in the longitudinal (x) direction, the data in the left sampling area are reversed and analyzed together with the data in the right sampling area. The profiles of the x -component of the velocity across the microchannel for cases A and B are plotted using solid lines with markers in Fig. 6. To compare the profiles for the different rarefaction conditions of cases A and B, the velocity was normalized by the positive maximum value $v_{x,\max}$, which was 2.1 m/s for case A and 2.6 m/s for case B. To relate the velocity profile to the flow structure inside the normalized by the maximum number density value n_{\max} , which was 7.3 nm^{-3} for case A and 8.5 nm^{-3} for case B, is plotted using broken lines. In Fig. 6, two peaks of the layered structure in the vicinity of the walls are observed from the number density profiles, which is similar to the density profile in the numerical study of dense gases.^{24–26} The z -positions of these layers are independent of the Knudsen number conditions, indicating that they are adsorption layers based on the

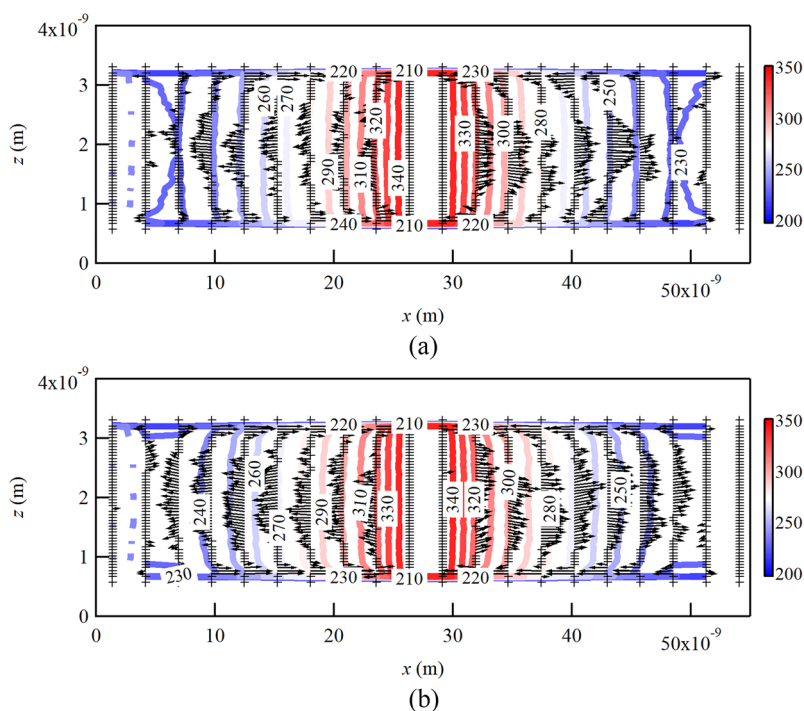


FIG. 4. Velocity vector plots with the temperature distribution shown in the contour lines for two cases with different rarefactions: (a) case A and (b) case B.

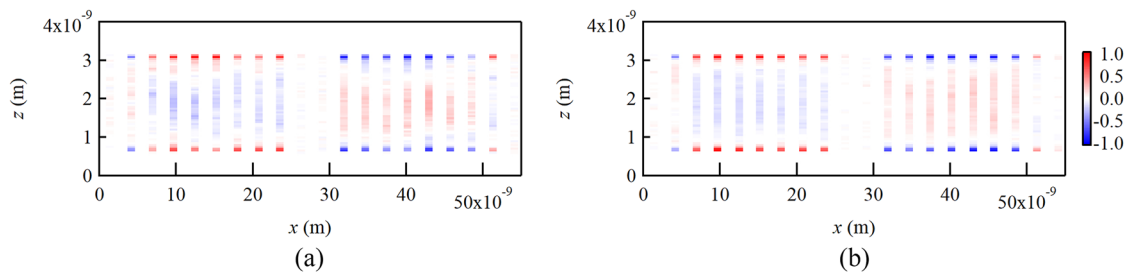


FIG. 5. The distribution of the product of number density and x-component of the velocity normalized by the maximum value for (a) case A and (b) case B.

interaction between the gas and surface. Gas molecules easily adsorb on a clean flat surface. These adsorption layers might be coming from the dense gas condition. The formation of the second adsorption layer can be observed in case A, which seems to be due to a high number density. For the velocity profiles, interestingly, the negative velocity, which is the thermal transpiration flow, appears near the wall, where the relative number density is large. The thermal transpiration flow appears to be induced inside the adsorption layers under the dense gas condition. Because the initial pressure distribution was very small, the thermal transpiration flow was not the result of the mass balance coming from the pressure driven flow, but it was considered to be induced by the temperature gradient.

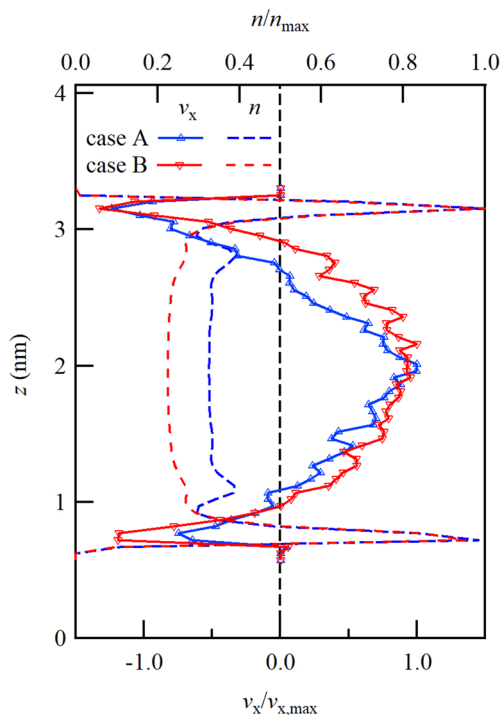


FIG. 6. Profiles of the x-component of velocity across the nanochannel averaged in two sampling areas compared between two cases with different rarefactions (case A in blue and case B in red). The number density profiles are also plotted.

C. Molecular motions near the channel wall

To check the characteristics of the two peaks of the number density profiles, the survival probability P_s ²⁷ was calculated. This probability was calculated using a ratio of a time-dependent number of molecules continuously existing in a certain region $N(t)$ to its initial value $N(0)$ as follows:

$$P_s = \frac{N(t)}{N(0)}. \quad (3)$$

Equation (3) represents the mobility of the molecules migrating between regions. Here, we divided the microchannel into eight slabs with a thickness of 0.34 nm in the height (z) direction. The slabs were the first and second adsorption layers on both top and bottom channel walls, and the bulk region was divided into four slabs. Because the four bulk regions produced similar results, the survival probabilities for the first and second adsorption layers and a bulk region are plotted in Fig. 7 using solid lines for case A and broken lines for case B. It is shown that the relaxation time of the survival probabilities in the first adsorption layers is larger than those in other regions. This result also indicates that gas molecules adsorbed and created a layer on the channel wall surfaces. For the smaller Knudsen number of case A, we can distinguish the second adsorption layer from the bulk, but it is quite difficult to recognize this for case B. The area of

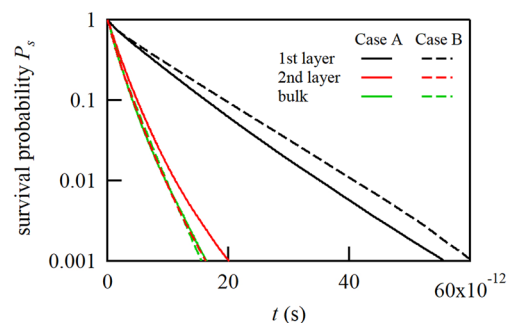


FIG. 7. The survival probabilities of gas molecules in the first (black) and second (red) adsorption layers; a bulk region (green) is plotted for cases A (solid lines) and B (dashed lines).

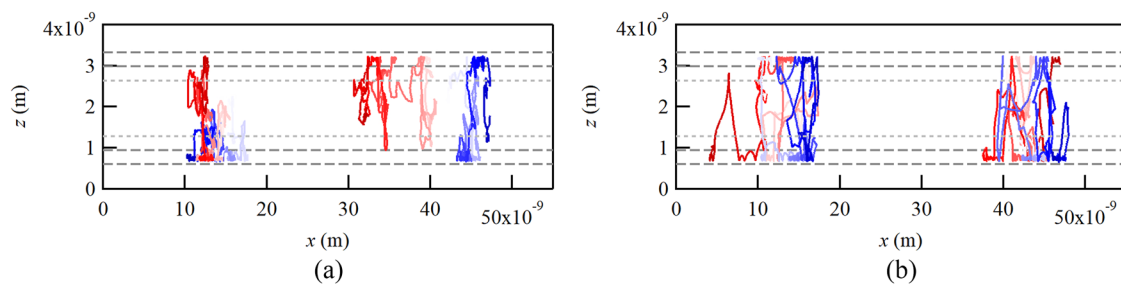


FIG. 8. Typical examples of gas molecular trajectories for (a) case A and (b) case B. The color of the trajectories becomes darker as time progresses. Blue trajectories are the molecules that are trapped for an extended time (36.4 ps and 31.2 ps for case A and 58.4 ps and 47.1 ps for case B) in the adsorption layer, and red trajectories are the molecules that remain for an extended time (22.4 ps and 19.5 ps for case A and 19.4 ps and 17.7 ps for case B) in the bulk region. The broken and dotted lines are the boundaries of the first and second adsorption layers.

the thermal transpiration flow in the velocity profile is larger for case A than case B (see Fig. 6), which is consistent with the existence of the second adsorption layer. According to the survival probability, the thermal transpiration flow is mainly induced in the adsorption layers.

To understand the thermal transpiration flow inside the adsorption layers, the trajectories of the gas molecules were investigated. The trajectory of the gas molecules that remained for an extended period in the adsorption layer was compared with those in the bulk. Typical examples of the trajectories of the gas molecules are shown in Fig. 8. Blue trajectories represent the molecules that are trapped for an extended period (36.4 ps and 31.2 ps for case A and 58.4 ps and 47.1 ps for case B) in the first adsorption layers, and red trajectories represent the molecules that remained in the bulk for an extended time without entering the first adsorption layer (22.4 ps and 19.5 ps for case A and 19.4 ps and 17.7 ps for case B). The position of the first adsorption layer was also plotted. As shown in Fig. 8, gas molecules traveled quite a long distance without collisions for the higher Kn condition of case B. For blue trajectories, gas molecules were trapped by the surface atoms, and they bounded and migrated on the surface. However, some molecules moved from the end to the center, i.e., from the cold to hot part, but some molecules moved in the opposite direction. There appeared no specific motions in any of the gas molecules for inducing the thermal transpiration flow. Gas molecules randomly migrated. Nonetheless, there would be a shift of the mean value in a specific direction based on the velocity distribution function, resulting in the thermal transpiration flow. This statistical feature is only the result of observing a vast number of gas molecules, however, and may be difficult to observe from a single molecular motion.

IV. CONCLUSION

Thermal transpiration flow through a 2D nanochannel was studied using MD simulation to investigate the flow structure. The nanochannel was simulated with the periodic boundary condition in all directions. Its temperature was controlled so that it was hot at the center and cold at both ends. The solid atoms of the channel wall were also controlled based on their positions by linearly

interpolating the temperature between the hot and cold temperature-controlled regions. By changing the width of the computational cell, two Knudsen number conditions, $Kn = 0.099$ and 0.30 , were examined while keeping the number of gas molecules approximately the same. To obtain the velocity vector distribution inside the nanochannel, simulations were carried out for 10 ns with a time step of 1 fs to reduce the statistical error. We successfully obtained the mean velocity distribution inside the nanochannel, showing the thermal transpiration flow in the vicinity of the channel wall with a pressure-driven counterflow at the center in the height direction even under the dense gas condition. The velocity profile across the nanochannel in the height direction was investigated using the number density profile. The number density profile indicated that there were adsorption layers on the channel wall, which was also verified from the survival probabilities of gas molecules in the slabs located in the height direction. There were two adsorption layers for the low Knudsen number condition and one for the high Knudsen number condition. The comparison of the two profiles suggested that thermal transpiration flow had been induced in the adsorption layer for both Knudsen number conditions under the dense gas condition.

ACKNOWLEDGMENTS

This study was partially supported by the Collaborative Research Project of the Institute of Fluid Science, Tohoku University. Numerical simulations were performed on the SGI Altix UV1000 and UV2000 and the Supercomputer system “AFI-NITY” at the Advanced Fluid Information Research Center, Institute of Fluid Science, Tohoku University. H.Y. acknowledges Dr. Pierre Perrier (Aix-Marseille University) for valuable discussions in the early stage of the study.

DATA AVAILABILITY

The data that support the findings of this study are available from the corresponding author upon reasonable request.

REFERENCES

- ¹G. Karniadakis, A. Beskok, and N. Aluru, *Microflows and Nanoflows: Fundamentals and Simulation* (Springer-Verlag, New York, 2005).
- ²Y. Sone, *Molecular Gas Dynamics: Theory, Techniques, and Applications* (Birkhäuser, Boston, 2007).
- ³F. Sharipov, *Rarefied Gas Dynamics: Fundamentals for Research and Practice* (Wiley-VCH, Weinheim, 2016).
- ⁴J. P. Hobson and D. B. Salzman, "Review of pumping by thermal molecular pressure," *J. Vac. Sci. Technol., A* **18**, 1758–1765 (2000).
- ⁵S. Colin, "Rarefaction and compressibility effects on steady and transient gas flows in microchannels," *Microfluid. Nanofluid.* **1**, 268–279 (2005).
- ⁶X. Wang, T. Su, W. Zhang, Z. Zhang, and S. Zhang, "Knudsen pumps: A review," *Microsyst. Nanoeng.* **6**, 26 (2020).
- ⁷S. McNamara and Y. B. Gianchandani, "On-chip vacuum generated by a micro-machined Knudsen pump," *J. Microelectromech. Syst.* **14**, 741–746 (2005).
- ⁸Y. Qin and Y. B. Gianchandani, "A fully electronic microfabricated gas chromatograph with complementary capacitive detectors for indoor pollutants," *Microsyst. Nanoeng.* **2**, 15049 (2016).
- ⁹B. T. Porodnov, A. N. Kulev, and F. T. Tuchevevov, "Thermal transpiration in a circular capillary with a small temperature difference," *J. Fluid Mech.* **88**, 609–622 (1978).
- ¹⁰M. Rojas-Cárdenas, I. Graur, P. Perrier, and J. G. Méolans, "Thermal transpiration flow: A circular cross-section microtube submitted to a temperature gradient," *Phys. Fluids* **23**, 031702 (2011).
- ¹¹H. Yamaguchi, M. Rojas-Cárdenas, P. Perrier, I. Graur, and T. Niimi, "Thermal transpiration flow through a single rectangular channel," *J. Fluid Mech.* **744**, 169–182 (2014).
- ¹²M. Rojas-Cárdenas, I. Graur, P. Perrier, and J. G. Méolans, "Time-dependent experimental analysis of a thermal transpiration rarefied gas flow," *Phys. Fluids* **25**, 072001 (2013).
- ¹³H. Yamaguchi, P. Perrier, M. T. Ho, J. G. Méolans, T. Niimi, and I. Graur, "Mass flow rate measurement of thermal creep flow from transitional to slip flow regime," *J. Fluid Mech.* **795**, 690–707 (2016).
- ¹⁴F. Sharipov and V. Seleznev, "Data on internal rarefied gas flows," *J. Phys. Chem. Ref. Data* **27**, 657–706 (1998).
- ¹⁵F. Sharipov and G. Bertoldo, "Poiseuille flow and thermal creep based on the Boltzmann equation with the Lennard-Jones potential over a wide range of the Knudsen number," *Phys. Fluids* **21**, 067101 (2009).
- ¹⁶H. Akhlaghi and E. Roohi, "Mass flow rate prediction of pressure-temperature-driven gas flows through micro/nanoscale channels," *Continuum Mech. Thermodyn.* **26**, 67–78 (2014).
- ¹⁷D. A. Lockerby, A. Patronis, M. K. Borg, and J. M. Reese, "Asynchronous coupling of hybrid models for efficient simulation of multiscale systems," *J. Comput. Phys.* **284**, 261–272 (2015).
- ¹⁸P. Wang, W. Su, and L. Wu, "Thermal transpiration in molecular gas," *Phys. Fluids* **32**, 082005 (2020).
- ¹⁹N. N. Nguyen, I. Graur, P. Perrier, and S. Lorenzani, "Variational derivation of thermal slip coefficients on the basis of the Boltzmann equation for hard-sphere molecules and Cercignani-Lampis boundary conditions: Comparison with experimental results," *Phys. Fluids* **32**, 102011 (2020).
- ²⁰G. Babac, N. Dongari, Y. Zhang, and J. M. Reese, "Thermal transpiration of nanoscale gas flow," *AIP Conf. Proc.* **1501**, 946–953 (2012).
- ²¹J. Francis T and S. P. Sathian, "Thermal transpiration: A molecular dynamics study," *AIP Conf. Proc.* **1628**, 901–908 (2014).
- ²²S. K. Prabha and S. P. Sathian, "Molecular-dynamics study of Poiseuille flow in a nanochannel and calculation of energy and momentum accommodation coefficients," *Phys. Rev. E* **85**, 041201 (2012).
- ²³W. Humphrey, A. Dalke, and K. Schulten, "VMD: Visual molecular dynamics," *J. Mol. Graphics* **14**, 33–38 (1996).
- ²⁴S. V. Nedeia, A. J. H. Frijns, A. A. van Steenhoven, A. P. J. Jansen, A. J. Markvoort, and P. A. J. Hilbers, "Density distribution for a dense hard-sphere gas in micro/nano-channels: Analytical and simulation results," *J. Comput. Phys.* **219**, 532–552 (2006).
- ²⁵L. Wu, H. Liu, J. M. Reese, and Y. Zhang, "Non-equilibrium dynamics of dense gas under tight confinement," *J. Fluid Mech.* **794**, 252–266 (2016).
- ²⁶Q. Sheng, L. Gibelli, J. Li, M. K. Borg, and Y. Zhang, "Dense gas flow simulations in ultra-tight confinement," *Phys. Fluids* **32**, 092003 (2020).
- ²⁷J. Suzuki, G. Kikugawa, T. Nakano, and T. Ohara, "Kinetic model for transport of liquid molecules in the solid-liquid interface region: A molecular dynamics view," *Mech. Eng. Lett.* **1**, 15-00353 (2015).